Rev.Adv.Mater.Sci. 16(2007) 80-87

EFFECT OF ARGON-NITROGEN MIXING GAS DURING MAGNETRON SPUTTERING ON TITANIUM INTERLAYER DEPOSITION WITH TiB_2 COATINGS ON HIGH SPEED STEEL

N. Panich[1], P. Wangyao[1], S. Hannongbua[1], P. Sricharoenchai[2] and Y. Sun[3]

[1] Metallurgy and Materials Science Research Institute, Chulalongkorn University, Phrayathai Rd., Pathumwan, Bangkok, 10330, Thailand
[2]Dept. of Metallurgical Engineering, Faculty of Engineering, Chulalongkorn University, Phrayathai Rd., Pathumwan, Bangkok, 10330, Thailand
[3] School of Engineering & Technology, De Montfort University, Leicester LE1 9BH, UK

Received: July 14, 2007

Abstract. It has been a common practice that in the deposition of a ceramic coating onto a substrate, a thin titanium interlayer is used to improve the adhesion between the coating and the substrate. But the structure and strength of the interlayer play an important role in determining the adhesion strength of the coating. This work involves the deposition of titanium diboride (TiB_2) based nanostructured coatings on high speed steel substrates. A titanium interlayer was applied by sputtering a titanium target in pure argon atmosphere and in argon-nitrogen gas mixtures to affect nitrogen doping of the interlayer. Structural and properties analysis revealed that various contents of nitrogen gas in argon-nitrogen gas mixture during deposition by magnetron sputtering has significant effect on the adhesion between the TiB_2 coating and the high speed steel substrate. There exists an optimum degree of nitrogen incorporation in the interlayer that results in the maximum enhancement in adhesion. The beneficial effect of nitrogen gas mixing is discussed in terms of the modified structure and increased hardness of the interlayer, which provides stronger support for mechanical loading.

1. INTRODUCTION

Titanium diboride, TiB_2, is a ceramic compound with a hexagonal crystal structure and possessing high hardness, good chemical stability, and good thermal and electrical conductivity. There have been increasing interests in fabrication of this material in thin film and coating forms for many potential applications, for example to combat wear, protective coatings, corrosion and tribological engineering components and particularly in material processing tools and dies [1-5]. Even though the structures and properties of sputter-deposited TiB_2 coatings have been studied by many investigators, the commercialization of TiB_2 coatings has been impeded mainly due to the difficulties in producing high quality coatings with good mechanical properties and coating adhesion suitable for industrial applications.

The major problem is that TiB_2 coatings are very brittle and usually have poor adhesion with metallic substrates, which is the main barrier for the industrial application of TiB_2 coatings. Recently, several attempts have been made to overcome these problems, for example by sputter cleaning the substrate [6], applying substrate bias during deposition [7,8], annealing after deposition [3,4,9], forming multilayer and composite coatings [10-12] and introducing nitrogen during deposition [13,14]. It has been a common practice that in the deposition of a ceramic coating onto a substrate, a thin titanium interlayer is used as a “glue” to improve the adhe-

Corresponding author: P. Wangyao, e-mail: panyawat@hotmail.com

Table 1. Deposition conditions.

Samples	Mode	Substrate cleaning	Deposition details	Percentage of N_2
No.1	Graded Ti-TiB_2	150 W 30 min	Ti 200 W 30 min, TiB_2 200 W 180 min	0
No.2	Graded Ti-TiB_2	150 W 30 min	Ti 200 W 30 min, TiB_2 200 W 180 min	10
No.3	Graded Ti-TiB_2	150 W 30 min	Ti 200 W 30 min, TiB_2 200 W 180 min	20
No.4	Graded Ti-TiB_2	150 W 30 min	Ti 200 W 30 min, TiB_2 200 W 180 min	33
No.5	Graded Ti-TiB_2	150 W 30 min	Ti 200 W 30 min, TiB_2 200 W 180 min	50

sion between the coating and the substrate. Genuinely, the use of a thin titanium interlayer has been found to considerably improve the adhesion of titanium nitride coatings produced by physical vapor deposition [15]. The role of the interlayer is considered to be twofold. First, the titanium interlayer acts as an oxygen getter for the substrate surface. This helps to decompose the native oxide film on the substrate surface and promote the adhesion between the coating and the substrate. Second, it serves as a compliance layer to accommodate the stress at the coating-substrate interface. Thus, the structure and strength of the interlayer play an important role in determining the adhesion strength of the coating.

This paper involves the deposition of TiB_2 based nanostructured coatings on high speed steel substrates. A titanium interlayer was applied by sputtering a titanium target in pure argon atmosphere and in argon-nitrogen gas mixtures to influence the interlayer. Structural and properties analysis revealed that argon-nitrogen gas mixture is beneficial in improving the adhesion between the TiB_2 coating and the high speed steel substrate.

2. EXPERIMENTAL PROCEDURE

High-speed steel (HSS) was chosen as substrates in this study. The commercial HSS, SECO WKE45 (Sweden) in fully hardened and tempered condition was cut into 12×12×3 mm pieces. The specimen's surface was manually ground and polished. The HSS substrates were then ultrasonically cleaned with acetone and ethanol before charging the deposition chamber. High-purity argon gas was then introduced into the chamber after it was evacuated to below $5 \cdot 10^{-4}$ Pa. The TiB_2 target (75 mm diameter and 5 mm thick) was powered in the radio frequency (RF) mode and the Ti target was powered in the direct current (DC) mode. The substrates were positioned near to the edge of the working table below the TiB_2 target. The substrates were stationary and the distance between the TiB_2 target and the substrate was fixed at 60 mm. All the experiments were conducted at a constant working pressure of 0.65 Pa, Ar gas flow rate of 20 sccm, varied nitrogen gas flow rates (see Table 1), a constant substrate temperature of 400 °C and a constant RF sputtering power (for TiB_2 target) of 200 W. A thin (about 50 nm) pure Ti interlayer was deposited first in all cases, by sputtering the Ti target for 30 min with a DC power of 200 W. Before deposition, the substrates were sputter-cleaned for 30 min to remove oxide layers or contaminants at the substrate surface. In addition, in order to avoid the formation of TiN compound during deposition of nitrogen-doped Ti interlayer, no substrate biasing during deposition was applied for all depositions. Table 1 summarizes the deposition details in this study.

The phase composition of the resultant coatings was examined by Rigagu X-ray diffractometer with Cu-Kα radiation. Crystallographic phases were deduced by comparing the experimental diffraction patterns with the standard JCPDS data. The morphology of surfaces and fractured cross-sections of the coatings were imaged using a field emission scanning electron microscope (FESEM), Jeol JSM 6340F. The coating thickness was measured by making a ball-crater on the coating surface using the Calotest machine manufactured by CSEM. A stainless steel ball of 25.4 mm diameter was used for cratering with a speed of 500 rpm for 240 s. The roughness of surfaces (R_a) was measured using an atomic force microscopy (AFM), Digital Instrument and the average roughness (R_a) values are listed in Table 2.

Table 2. Properties of resultant coatings.

Samples	Percentage of N_2	Coating Thickness (micron)	R_a (nm)	Hardness (GPa)	Reduced modulus (GPa)	Critical load *Lc* (mN)
No.1	0	1.90	6.95	31.6	321.3	1,089.1
No.2	10	1.85	1.87	35.6	316.2	1,784.5
No.3	20	1.87	1.62	33.3	355.8	1,352.4
No.4	33	1.89	1.51	33.2	332.7	1,446.1
No.5	50	1.92	0.81	29.9	310.5	1,387.5

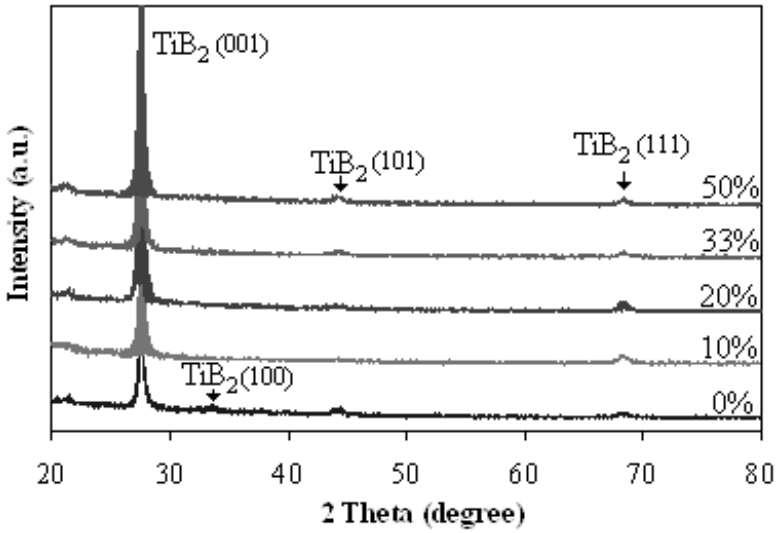

Fig. 1. XRD patterns of all samples.

Nanoindentation test was performed using the NanoTest™ instrument (Micro Materials Limited, UK), with a Berkovich diamond indenter. All experiments were performed at a constant loading and unloading rate of 0.05 mN/s and to a penetration depth of 50 nm. The unloading curves were used to derive the hardness and reduced modulus values by the analytical technique developed by Oliver and Pharr [16]. The reported hardness and modulus values are the average of 10 measurements. The microscratch test was performed using the multipass microscratch mode available in the NanoTest™ device with a diamond indenter topped with a conical with spherical end form of 25 μm in radius. A new test method was employed in this work, as described by Xia *et. al.* [17].

3. RESULTS AND DISCUSSION

3.1. Structural characterization of resultant coatings

Fig. 1 shows the X-ray diffraction patterns recorded for all five samples listed in Table 1. Each pattern shows several broad reflection peaks corresponding to the hexagonal TiB_2 structure. The dominant peak is (001), which indicates that the basal plane of TiB_2 is preferentially oriented parallel to the substrate surface in all samples. The degree of such preferred orientation seems to increase with increasing content of nitrogen in argon-nitrogen gas mixture, as evident from the increased relative intensity of the (001) peak. Such a (001) texture may account for the observed higher hardness of the coatings, since TiB_2 coatings with (001) orienta-

tion is known to yield the highest hardness as compared with TiB_2 coatings with other orientation [18]. The broadness of the reflection peaks indicates the nanocrystalline nature of the coating structure, as further confirmed by FESEM examination (Fig. 2). No reflection peaks corresponding to TiN phase were observed in the X-ray diffraction patterns, indicating that under the present argon-nitrogen gas mixture conditions did not lead to TiN compound formation, and nitrogen atoms are dissolved in the α-Ti lattice to form solid solution.

The morphologies of the as-deposited coating surfaces and fractured cross-sections were examined under FESEM, as illustrated in Fig. 2 for sample 1. Similar morphological features were also observed for other coatings. In all cases, the coating surface is populated with granular grains with typical size less than 30 nm. The virtual grains are formed from many nanoclusters and they have well-defined boundaries with the others. Some pores of less than 10 nm size could be observed at virtual grain boundaries. Regarding the fractured cross-section (Fig. 2b), it is obvious that a thin Ti interlayer could be observed in all samples. From Fig. 2b, it can also be seen that the resultant coating exhibits a columnar structure, which is typical of sputter deposition at relatively low adatom energies and limited mobility.

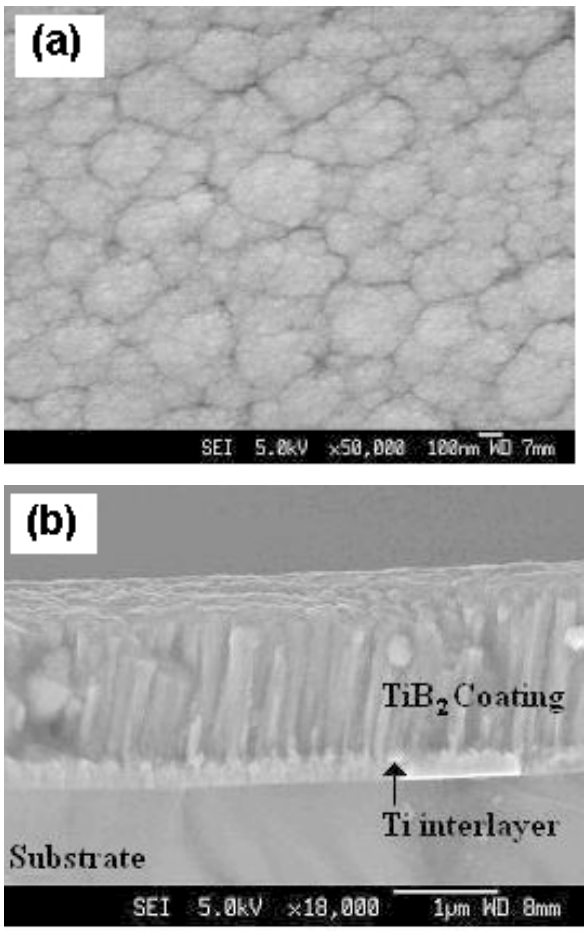

Fig. 2. FESEM images showing the surface morphology and fractured cross-sectional morphology of TiB_2 coatings (sample 1).

3.2. Surface roughness

The surface morphology and roughness values were measured by AFM for the coatings deposited on silicon substrates under the same conditions as listed in Table 1. In this study, silicon wafer was used as a substrate material for AFM measurements due to the beginning smoothness with an average roughness (R_a) of about 0.15-0.20 nm. The surfaces of the resultant coatings deposited on silicon substrates were found to be quite smooth and homogenous, with R_a at the nano-scale, as listed in Table 2. It can be clearly seen from Table 2 that argon-nitrogen gas mixture is very effective in reducing the surface roughness of the subsequent TiB_2 coating. For example, the R_a value of TiB_2 coating surface was reduced from 6.95 to 1.87 nm and further to 0.81 nm with increasing nitrogen content in argon-nitrogen gas mixture. This demonstrates the beneficial effect of argon-nitrogen gas mixture in maintaining the smoothness of the substrate surface, which is important for many practical applications.

Fig. 3 shows the AFM images recorded for all the coating surfaces. All coatings exhibit similar surface morphological features, characterized by the densely populated conical projections. But the number and individual size of these conical projections vary with the nitrogen content in argon-nitrogen gas mixture: with increasing nitrogen content, the number of projections increases and the size of individual projects decreases. These are in good agreement with the R_a roughness values measured for the coating surfaces.

3.3. Coating hardness

In order to assess the intrinsic mechanical properties of the coatings i.e. hardness and reduced modulus, all specimens were indented at 50 nm penetration depth to avoid any possible effect from the substrate during the indentation process. The

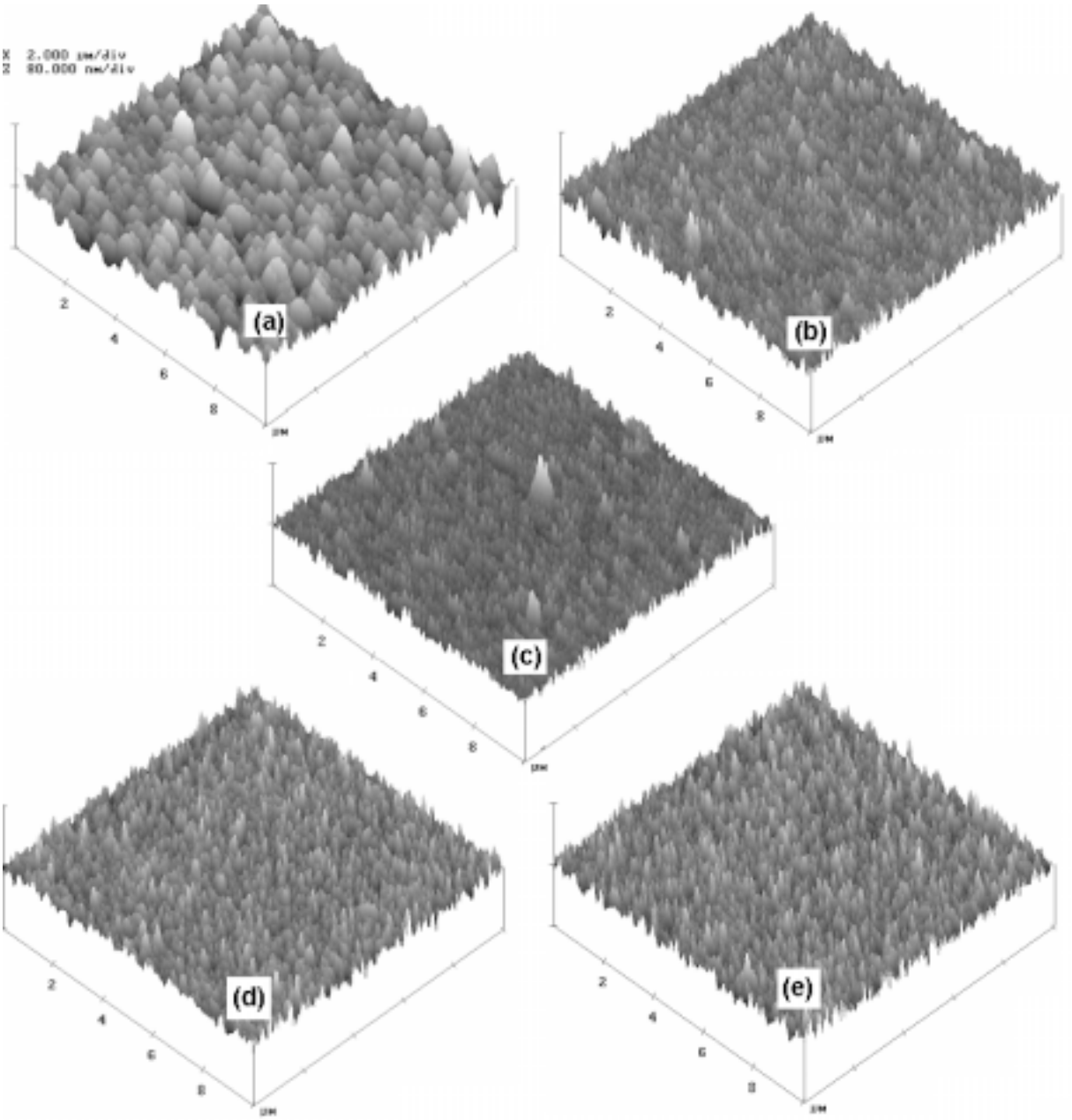

Fig. 3. AFM images showing the average surface roughness (R_a) of all tested samples
(a) Sample No. 1., (b) Sample No. 2., (c) Sample No. 3., (d) Sample No. 4., and (e) Sample No. 5.

hardness and reduced modulus values of all TiB_2 coatings, measured by nanoindentation, are summarized in Table 2.

Fig. 4 shows the relationship between coating hardness and nitrogen content in argon-nitrogen gas mixture (represented by N_2 % in the sputtering atmosphere). The hardness values of the Ti interlayers were also measured as a function of nitrogen content in argon-nitrogen gas mixture. This was done on a separate series of samples deposited with Ti interlayers only without the subsequent TiB_2 coating deposition. An important observation that can be made from Fig. 4 is that without nitrogen doping, the pure Ti interlayer is very soft, with

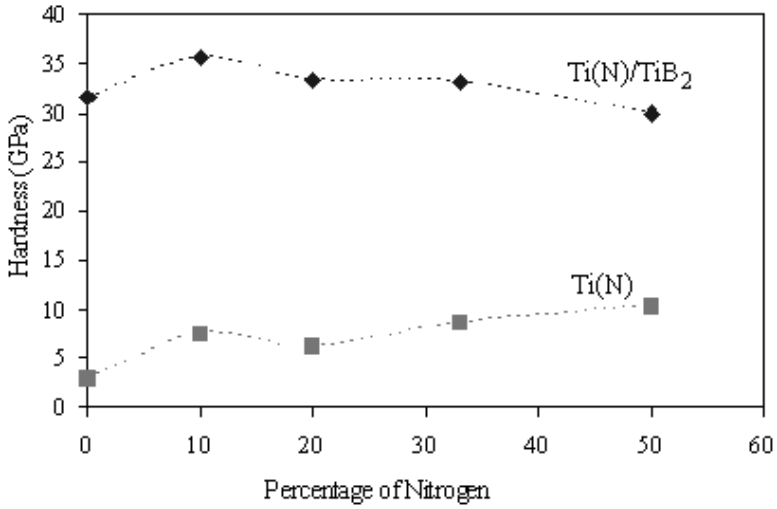

Fig. 4. The relationship between the coating hardness and percentage of nitrogen.

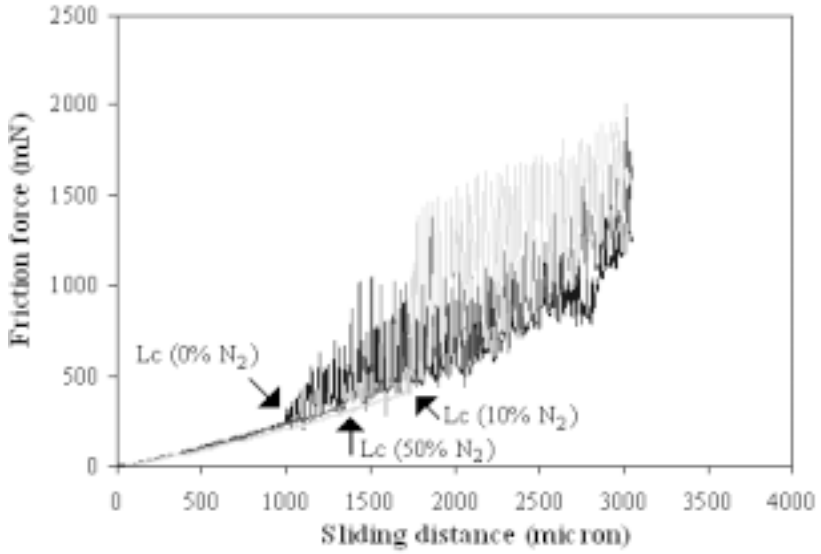

Fig. 5. Friction versus load curves for selected coatings.

hardness value around 2.5 GPa, and nitrogen mixing is effective in enhancing the hardness and strength of the interlayer. There is a general trend that the hardness of the Ti interlayer increases with increasing degree of nitrogen doping. This is obviously due to the dissolution of nitrogen in the α-Ti lattice, causing solid solution hardening in the interlayer. Such an increased interlayer strength may account for the observed enhancement in TiB_2-substrate adhesion as discussed later.

From Fig. 4, it can also be seen that the hardness of the TiB_2 coating first increases with increasing nitrogen content in argon-nitrogen gas mixture, and then decreases with further increased nitrogen content. The hardness peaked at 10% N_2 may be attributed to the increased hardness of the Ti interlayer and the enhanced (001) preferred orientation of the TiB_2 coating (Fig. 1), as TiB_2 coating with (001) orientation is known to yield the highest hardness as compared with TiB_2 coatings with other orientations. However, the reasons associated with the decrease in TiB_2 hardness with further increased nitrogen content are not fully understood. One possible reason may arise from the embrittlement of the interlayer resulting from too much nitrogen incorporation.

3.4. Coating-substrate adhesion

Fig. 5 shows typical friction versus scratching load curves measured during the microscratch test. Each friction curve can be divided inter two characteristic regimes: a smoothly increased region, followed by a sudden increase and then a large fluctuating region. As confirmed by microscopic examination, the sudden change in friction during scratch test is due to coating adhesive failure, and the corresponding load (L_C) is thus used as a measure of the adhesion strength of the TiB_2 coating to the HSS substrate. Table 2 also summarises the L_C values for all the coatings studies in this work. Clearly, nitrogen content in argon-nitrogen gas mixture can significantly enhance the TiB_2-HSS adhesion, with 10% N_2 in argon-nitrogen gas mixture is the most effective. This is another important observation made in this work, since coating-substrate adhesion is critical in many practical applications.

The observed enhancement in adhesion strength can be attributed to the increased strength of the nitrogen influenced on Ti interlayer. As discussed previously, the titanium interlayer serves as an oxygen getter to decompose the native oxide film on the substrate surface, thus promoting adhesion between the coating and the substrate. The argon-nitrogen gas mixture does not significantly change the chemical nature of α-Ti, because no TiN compound is formed and nitrogen is dissolved in the α-Ti lattice. It is thus expected that the Ti interlayer, influenced by argon-nitrogen gas mixture, also plays a similar role as an oxygen getter. In addition, the interlayer also provides compliance for the hard and brittle TiB_2 coating and helps to accommodate interfacial stresses through plastic deformation. However, if the interlayer is too soft, such as a pure Ti interlayer, it will deform too easily and provide less support to the TiB_2 coating.

With argon-nitrogen gas mixture, the Ti interlayer becomes stronger and thus can provide increased support to the TiB_2 coating, leading to enhanced adhesion strength. But, with further increasing nitrogen content, the interlayer becomes too strong and brittle to accommodate the interfacial stresses, leading to the observed reduction in adhesion strength. The argon-nitrogen gas mixture with 10% N_2 seems to produce the optimum combination of strength and compliance for adhesion enhancement in the present deposition conditions.

4.CONCLUSIONS

From the experimental results under the present deposition conditions, it can be concluded that the Ti interlayer under argon-nitrogen gas mixture condition has the following beneficial effects on the structures and properties on sputtered TiB_2 coatings:

(1) It can increase the hardness and strength of the interlayer due to nitrogen dissolution in the α-Ti lattice.
(2) It can enhance the (001) preferred orientation of the subsequent TiB_2 coating.
(3) It is effective in reducing the surface roughness of the TiB_2 coating.
(4) It can significantly enhance the TiB_2 coating-HSS substrate adhesion strength, with argon-nitrogen gas mixture of 10% N_2 showing the optimum enhancement.

REFERENCES

[1] J. Chen and J. A. Barnard // *Materials Science and Engineering A* **191** (1995) 233.
[2] E. Matrubara, Y. Waseda, S. Takeda and Y. Taga // *Thin Solid Films* **186 (**1990) L33.
[3] R. Wiedemann, H. Oettel and M. Jerenz // *Surface Coating and Technology* **97** (1997) 313.
[4] B. Todorovic, T. Jokic, Z. Rakocevic, Z. Markovic, B. Gakovic and T. Nanadovic // *Thin Solid Films* **300** (1997) 272.
[5] M. Berger // *Surface Engineering* **18** (2002) 219.
[6] P. Losbichler, C. Mitterer, P. N. Gibson, W. Gissler, F. Hofer and P. Warbichler // *Surface Coating and Technology* **94-95 (**1997) 297.
[7] M. Berger, L. Karlsson, M. Larsson and S. Hogmark // *Thin Solid Films* **401 (**2001) 179.
[8] N. Panich, P. Wangyao, S. Hannongbua, P. Sricharoenchai and Y. Sun // *Journal of Metals, Materials and Minerals* **16/1** (2006) 45.
[9] N. Panich, P. Wangyao, S. Hannongbua, P. Sricharoenchai and Y. Sun *// High Temperature Materials and Processes* **25/5-6** (2006) 285.
[10] N. Panich, P. Wangyao, S. Hannongbua, P. Sricharoenchai and Y. Sun *// Reviews on Advanced Materials Science* **13** (2006) 117.
[11] J. L. He, S. Miyake, Y. Setsuhara, I. Shimizu, M. Suzuki, K. Numata and H. Saito // *Wear* **249** (2001) 498.
[12] L. Ju-Wan, L. Jung-Joong, H. Ann and K.-T. Rie // *Surface Coating and Technology* **174-175** (2003) 720.

[13] J. F. Pierson, E. Tomasella and Ph. Bauer // *Thin Solid Films*, **408** (2002) 26.
[14] Y. Qiaoqin, Z. Lihua, W. Lijun and D. J. Haiqing // *Material Science Letters* **15** (1996) 11.
[15] S. J. Bull, P. R. Chalker, C. F. Ayres and D. S. Rickerby // *Materials Science and Engineering A* **139** (1991) 71-78.
[16] W. C. Oliver and G. M. Pharr // *Journal of Materials Research* **7** (1992) 1564.
[17] J. Xia, C. X. Li, H. Dong and T. Bell // *Journal of Materials Research* **19 (**2004) 291.
[18] H. Holleck // *Journal of Vacuum Science and Technology A* **4** (1986) 2661.